Voxel based adaptive spatio-temporal modelling of perfusion cardiovascular MRI

Volker J Schmid

***Abstract*—Contrast enhanced myocardial perfusion MRI is a promising technique, providing insight into how reduced coronary flow affects the myocardial tissue. Stenosis in a coronary vessel leads to reduced myocardial blood flow, but collaterals may secure the blood supply of the myocardium, with altered tracer kinetics. Due to a low signal-to-noise ratio, quantitative analysis of the signal is typically difficult to achieve at the voxel level. Hence, analysis is often performed on measurements that are aggregated in pre-defined myocardial segments, that ignore the variability in blood flow in each segment.**

The approach presented in this paper uses local spatial information that enables one to perform a robust analysis at the voxel level. The spatial dependencies between local response curves are modelled via a Hierarchical Bayesian Model. In the proposed framework, all local systems are analyzed simultaneously along with their dependencies, producing a more robust context-driven estimation of local kinetics. Detailed validation on both simulated and patient data is provided.

I. Introduction

First-pass perfusion cardiovascular Magnetic Resonance Imaging (MRI) provides valuable insight into how coronary artery and microvascular diseases affect myocardial tissue. It is commonly used with drug-induced stress to identify tissue with restricted myocardial blood flow due to obstructive coronary lesions. Intra-coronary collaterals, *i.e.*, arteries and arterioles, which interconnect major coronary artery branches, can function as natural bypass vessels in the myocardium. Hence, myocardial perfusion imaging plays a major role in the evaluation of ischaemic heart disease beyond situations where there have already been gross myocardial damages such as acute infarction or scarring [1]. It allows the understanding of micro-circulation in the myocardial tissue and myocardial angiogenesis [2].

Analysis of myocardial perfusion MRI is typically performed via deconvolution of the myocardial signal response with an Arterial Input Function (AIF) measured in the left ventricular (LV) blood pool. Due to low signal-to-noise ratio (SNR), standard deconvolution algorithms tend do be unstable for this problem. One approach to solve this problem is to increase the SNR by aggregating data in pre-defined regions of interest. A standard technique is to use myocardial segments. A standardized definition of myocardial segments was given by the Cardiac Imaging Committee of the Council on Clinical Cardiology of the American Heart Association [3]. However, by aggregating data on segment level, information on local variability of perfusion is lost.

Volker J Schmid is with the Department of Statistics, Ludwig-Maximilians-University Munich, 80539 Munich, Germany. He is supported by the LMUinnovative project BioMed-S: Analysis and Modelling of Complex Systems.

Voxel level deconvolution of the signal and input function is not possible without further constraints. For example, Goldstein *et al.* [4] made assumptions on the shape of residue curves in order to gain more robust estimates of Maximum Blood Flow (MBF). Jerosch-Herold *et al.* [5] proposed a model-free analysis, where the impulse response function is assumed to be a unknown smooth function, *i.e.*, is modelled by a B-Spline. The numerical stability is improved by assuming a smoothness constraint or penalty on the spline parameters, an approach which is also known as penalty splines or P-Splines [6]. Jerosch-Herold *et al.* determined the optimal value of the smoothing parameter with the L-curve method [7], however, this can also be done using cross validation [8] or in a Bayesian framework [9]. However, the algorithm proposed in [5] is still only feasible for data aggregated in segments or other regions of interest.

Instead of using a fixed smoothing parameter, we propose to allow time-varying smoothing for a more flexible shape of the response function. In order to keep numerical stability, we use a stricter penalty, *i.e.*, second-order differences instead of first-order differences. Time varying smoothing means that a vector of smoothing weights has to be estimated. This is only feasible in a Bayesian framework, where the smoothing weights can be estimated simultaneously along with the B-spline parameters. Due to the flexibility of the adaptive approach in dealing with rapid changes in the response function Bayesian P-Splines have received recent attention in both Dynamic contrast-enhanced MRI (DCE-MRI) [10] and myocardial perfusion MRI [11].

However, our results show that this approach in general is still not numerically stable for a voxel-by-voxel analysis. Hence, we propose to introduce spatial information into the deconvolution algorithm. Spatial information is inherent in images and is frequently used in image processing for denoising or segmentation [12]. Recently, it has been also exploited for dynamic medical images, *e.g.*, in functional MRI [13]–[15], ultrasound perfusion imaging [16], DCE-MRI [17], and diffusion tensor imaging [18]. For perfusion cardiovascular MRI a spatial approach was also proposed previously, however, not on voxel level, but at the myocardial segment level [19].

The assumption in these approaches is that the voxel grid is arbitrary and has no physical meaning. That is, adjacent voxel have similar tissue. One standard approach to model such spatial information is the Gaussian Markov Random Fields (GMRF) [20]. GMRFs are defined by specifying local neighborhoods, from which a global network of dependency is derived. This allows the algorithm to "borrow strength" from adjacent voxels for parameter estimation. Compared to

an independent voxel-by-voxel analysis additional information can be used and, hence, a more robust estimation is derived.

However, the assumption of smoothness may not always be correct. Typical medical images have some regions where tissue intensity surface "is smooth", *i.e.*, the intensities are homogeneous, in our example well-perfused healthy tissue. There are, however, also structural boundaries and regions with other distinct features, for example the edge between healthy and diseased tissue. Therefore, edge-preserving algorithms are necessary for medical images.

We adopt the idea of time-varying smoothing for spatial structures. That is, we use a locally adaptive smoothing approach [9], [17]. Spatial smoothing weights will be estimated from the data. Again, by using the Bayesian framework, estimation of spatial smoothing weights will be done simultaneously with the estimation of B-spline parameters, and the time-varying smoothing weights. Due to the high number of parameters, the only feasible way for optimization is a Markov chain Monte Carlo (MCMC) algorithm.

This paper proposes a spatio-temporal model, which allows robust quantitative analysis of perfusion cardiovascular MRI on voxel level. We will present the local B-Spline model adapted from [5], time-varying and adaptive spatial smoothing and the combination of these ideas, which we call the adaptive spatio-temporal model. The proposed model will be evaluated on simulated data and an *in vivo* data set. We will describe how estimates of MBF can be derived from the MCMC results and how the full Bayesian framework can help to assess the accuracy of parameter estimation. Results for the evaluation on simulated and *in vivo* data will be given in Section III, followed by a discussion.

II. Theory and Methods

A. Local B-Spline model

In each voxel i, the observed signal intensity Y_{it} at time t is the unknown true signal intensity $S_i(t)$ plus an observation error ϵ_{it}. We assume a Gaussian observation error with variance σ_i^2,

$$\epsilon_{it} \sim \mathrm{N}(0, \sigma_i^2) \text{ for all } i, t, \tag{1}$$

where N is the Gaussian distribution. In the Bayesian framework, we use a relatively flat prior for the unknown variance of the observation error, $\sigma_i^2 \sim \mathrm{IG}(a, b)$ for all i, with $a = 1, b = 10^{-3}$, where IG is the Inverse Gamma distribution.

In general, the true signal intensity is the convolution of the AIF $A(t)$, *i.e.*, the mean signal intensity in the LV blood pool, and a response function $f(t)$ [2]

$$S_n(t) = \int_0^t A(t-u) f_n(u) du. \tag{2}$$

After discretization at time points $t_1, \ldots, t_T$,

$$S_{it_j} = \sum_{l=1}^{T} A(t_j - t_l) f_i(t_l) \Delta t = \sum_{l=1}^{T} A_{jl} f_i(t_l), \tag{3}$$

where Δt represents the sampling interval of the dynamic series and the matrix $\boldsymbol{A} = (A_{ij})_{i=1,\ldots,T;j=1,\ldots,T}$ is a convolution operator [5]. We assume the response to be a smooth function and use a B-spline representation for $f_i(t)$,

$$f_i(t_j) = \sum_{p=1}^{P} \beta_{ip} B_{pj}, \tag{4}$$

where $\boldsymbol{B}$ is a $T \times P$ design matrix of $4th$ order B-splines, $\boldsymbol{\beta}_i$ represents the spline regression parameter vector for voxel i, and P is the number of basis splines. In vector notation, Eqn. 3 and Eqn. 4 are reduced to

$$\boldsymbol{S_i} = \boldsymbol{A f}_i = \boldsymbol{AB\beta}_i = \boldsymbol{D\beta}_i, \tag{5}$$

where $\boldsymbol{D} = \boldsymbol{AB}$ is the discrete convolution of the AIF with the B-Spline polynomials. Hence, the local model for voxel i may be written as

$$\boldsymbol{Y}_i = \boldsymbol{D\beta}_i + \boldsymbol{\epsilon}_i. \tag{6}$$

B. Temporal constraints

A typical constraint on $\boldsymbol{\beta}$ is a first or second order difference in the temporal dimension [5], [10]. In a Bayesian framework, this constraint is expressed as an *a priori* distribution [21]. This is also known as a "random walk" prior. We use second order differences,

$$\beta_{ip} \sim \mathrm{N}\left(2\beta_{i,p-1} - \beta_{i,p-2}, \tau_p^2\right) \quad \text{for all } p = 3, \ldots, P. \tag{7}$$

with τ_p^2 a time-varying smoothing parameter. In contrast to traditional approaches, the smoothing parameter τ_p^2 is specific for each difference. In total, we have $P - 2$ time-varying smoothing parameters.

The joint *a priori* distribution of $\boldsymbol{\beta}_{i\bullet} = (\beta_{i1}, \ldots, \beta_{iP})$ can be expressed as

$$\boldsymbol{\beta}_{i\bullet} \sim \mathrm{N}_P(0, \boldsymbol{R}^{-1}), \tag{8}$$

where N_P is the multivariate Gaussian distribution of dimension P, and $\boldsymbol{R}$ denotes the "precision matrix" (pseudo-inverse of the covariance matrix) of the random walk. The precision matrix includes the time-varying smoothness parameters. For *a priori* distribution for the time-varying smoothness parameters we use independent Inverse Gamma distributions [9]

$$\tau_p^2 \sim \mathrm{IG}(c, d) \text{ for all } p = 3, \ldots, P,$$

with parameters $c = d = 1$. This implies a smooth, but flexible shape of the response function.

C. Spatio-temporal constraints

The approach described in the previous section can be used to analyze data on voxel-by-voxel level, but it can also be used to analyze data aggregated in myocardial segments. We will now explore a way to add spatial information to the local penalized B-Spline model.

We assume that adjacent voxel share tissue, and, hence, their response functions have similar shapes. We account for cases where adjacent voxels do not have a similar response function – due to an "edge" in the tissue – by estimating locally adaptive smoothing weights along with the response function. We use a GMRF as a stochastic constraint on the spline regression parameters of adjacent voxels.

A GMRF is defined by the probability density function (pdf) of parameter β_{ip} given the parameters of its "neighbourhood" ∂_i, *i.e.*, all voxel adjacent to i. The conditional (pdf) is

$$\beta_{ip}|\boldsymbol{\beta}_{\partial_i p} \sim \mathrm{N}\left(\frac{\sum_{j\in\partial_i}\nu_{\{ij\}}\beta_j}{\sum_{j\in\partial_i}\nu_{\{ij\}}}, \left(\sum_{j\in\partial_i}\nu_{\{ij\}}\right)^{-1}\right) \quad (9)$$

for each i, p. Due to the relatively large gaps between slices in myocardial perfusion MRI we define neighbourhoods only within a slice.

Similar to adaptive temporal smoothing using penalized splines, there is no global smoothing weight, but spatially adaptive smoothing weights. A spatial smoothing parameter $\nu_{\{ij\}}$ is used for each pair $\{ij\}$ of adjacent voxel and quantifies the similarity of the response functions of both voxel. A low value of $\nu_{\{ij\}}$ indicates large differences in the shape of the response functions of voxel i and j, hence, an edge between i and j. *A priori*, the similarity between voxels is unknown. Hence, we estimate $\nu_{\{ij\}}$ simultaneously along with the response functions. In the Bayesian framework this is done by specifying a prior distribution. Here, we use independent Gamma distributions [9]

$$\nu_{\{ij\}} \sim \mathrm{Ga}(e, f) \text{ for all } \{i, j\}$$

with hyper parameters $e = f = 1$.

The joint *a priori* distribution of the spatial constraint per knot p is

$$\boldsymbol{\beta}_{\bullet p} \sim \mathrm{N}_N\left(0, \boldsymbol{Q}^{-1}\right), \quad (10)$$

where $\boldsymbol{Q}$ is the precision matrix of a Gaussian Markov random field [20] including the spatial distribution parameters $\nu_{\{ij\}}$. We now have to combine the *a priori* constraints in Eqn. 8 and Eqn. 10. This can be done via the Kronecker matrix sum of both precision matrices [22]. That is, the joint prior of $\boldsymbol{\beta}$ is

$$\boldsymbol{\beta} \sim \mathrm{N}_{N\cdot P}\left(0, ((\boldsymbol{Q}\otimes\boldsymbol{I_P}) + (I_N\otimes\boldsymbol{R}))^{-1}\right) \quad (11)$$

where $\boldsymbol{I}_N$ is the identity matrix with dimension $N \times \mathrm{N}$ and $\otimes$ is the Kronecker matrix product.

D. Bayesian results

For parameter estimation, we use a full Bayesian framework. That is, we draw conclusions only from the joint posterior pdf $p(\boldsymbol{\beta}, \boldsymbol{\tau^2}, \boldsymbol{\nu^2}, \boldsymbol{\sigma^2}|\boldsymbol{Y})$ given by Bayes' formula

$$p(\boldsymbol{\beta}, \boldsymbol{\tau^2}, \boldsymbol{\nu^2}, \boldsymbol{\sigma^2}|\boldsymbol{Y}) = \frac{\ell(\boldsymbol{Y}|\boldsymbol{\beta}, \boldsymbol{\sigma^2})p(\boldsymbol{\beta}|\boldsymbol{\tau^2}, \boldsymbol{\nu^2})p(\boldsymbol{\tau^2})p(\boldsymbol{\nu^2})p(\boldsymbol{\sigma^2})}{\int \ell(\boldsymbol{Y}|\boldsymbol{\beta}, \boldsymbol{\sigma^2})p(\boldsymbol{\beta}|\boldsymbol{\tau^2}, \boldsymbol{\nu^2})p(\boldsymbol{\tau^2})p(\boldsymbol{\nu^2}p(\boldsymbol{\sigma^2}))d\boldsymbol{\beta}d\boldsymbol{\nu^2}d\boldsymbol{\tau^2}d\boldsymbol{\sigma^2}}$$

where $\ell(\boldsymbol{Y}|\boldsymbol{\beta}, \boldsymbol{\sigma^2})$ is the likelihood of the data given the model parameters, see Eqn. 6, $p(\boldsymbol{\beta}|\boldsymbol{\tau^2}, \boldsymbol{\nu^2})$ is the prior pdf of the spline regression parameters as specified in Eqn. 11, $p(\boldsymbol{\sigma^2})$ is the prior pdf of the variance of the observation error, and $p(\boldsymbol{\tau^2})$ and $p(\boldsymbol{\nu^2})$ are the prior pdf of the time-varying and the locally adaptive spatial smoothing parameters, resp.

Parameter inference is based on an MCMC algorithm [23] which produces a random sample whose distribution is equal to the posterior pdf. From these samples, we can compute point estimates along with intervals to evaluate the uncertainty of the estimates. Here, we use the median of the posterior pdf as point estimates and the interquartile range (IQR) of the computed sample in order to quantify the uncertainty in parameter estimation. The quartile range $IQR(x)$ is defined as

$$IQR(x) = q_{0.75}(x) - q_{0.25}(x) \quad (12)$$

where $q_p(x)$ is the p-quantile of the sample x.

In the MCMC algorithm β, σ^2, and τ^2 can be updated using Gibbs steps. That is, values are updated by drawing a random number from the respective full conditional distribution; a multivariate Gaussian distribution for β, and independent Gamma distributions for σ^2, and τ^2. We use efficient algorithms for sampling from multivariate Gaussians with sparse precision matrices [20], using the `Matrix` package [24] in the statistical software `R` [25]. The adaptive spatial smoothing weight ν^2 can, however, only be updated by a Metropolis-Hastings step, as the full conditional distribution of a single ν_{ij}^2 actually includes the product of the non-negative eigenvalues of the matrix Q. Brezger *et al.* [9] developed an algorithm for efficient sampling of spatial adaptive GMRF with independent identical distributed priors for an application in functional MRI. We use this algorithm to update the spatial smoothing weights and refer to [9] for further reading.

E. Simulation studies

For numerical validation, a set of myocardial perfusion images was simulated. To gain realistic simulations, we extracted response functions in a scan under stress from a patient with reduced perfusion in the lateral segments of all slices, *i.e.*, in the area of the left circumflex coronary artery (LCX), and slightly reduced perfusion in the basal inferoseptal, basal and mid inferior segments. From the extracted response functions and the observed input function, we simulated voxel-wise signal as follows.

For simulation A, we smoothed the response functions derived above in order to suppress noise, see top left of Fig. 1. Here, we assume that perfusion, *i.e.*, MBF is spatially smooth. Afterwards, white noise was added to the signal in each voxel at four levels (SNR = $4.25, 3, 2.12, 1.5$).

For simulation B, standard myocardial segments were used. Response functions derived above were averaged per segment. The averaged segment response function was then assigned to each voxel in the segment, see top left of Fig. 2. We assume that the myocardial perfusion is equal for each voxel within a segment. Again, white noise was added at four levels to the simulated signal (SNR = $4.25, 3, 2.12, 1.5$).

Each simulation was repeated 50 times to evaluate the reliability of the proposed approach. To evaluate the simulation studies, for each simulated data set we compare true and estimated MBF derived by the approaches mentioned above via the mean squared error (MSE). For the segment approach, estimated MBF values per segment where assigned to each voxel in a segment. The MSE was computed as

$$MSE = \sum_{i=1}^{N}\left(MBF_i^{true} - \widehat{MBF}_i\right)^2$$

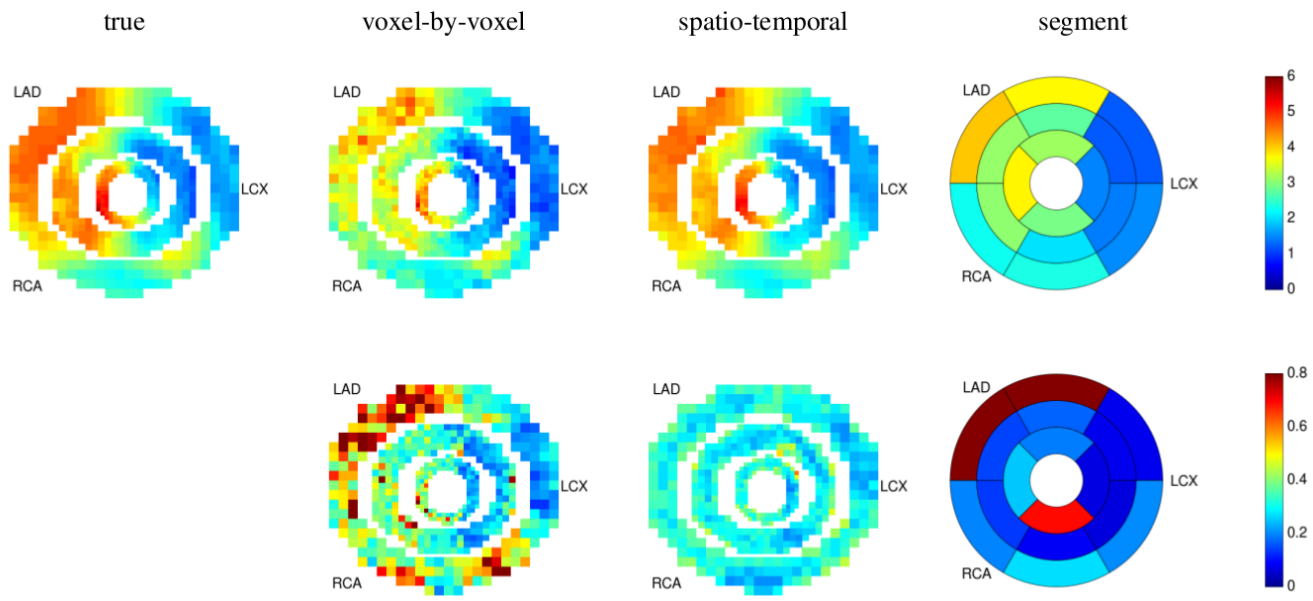

Fig. 1. Top row: True and estimated MBF values for one simulation run (SNR=3) of simulation A. Bottom row: IQR of estimated MBF for all three approaches.

TABLE I
SIMULATION A: MEAN SQUARED ERROR OF MBF; MEDIAN AND STANDARD DEVIATION (IN BRACKETS) OVER 50 SIMULATIONS, AT FOUR DIFFERENT NOISE LEVELS FOR ALL THREE APPROACHES.

SNR	4.25	3.00	2.12	1.50
segment	0.5817 (0.05979)	0.6789 (0.08223)	0.9028 (0.08494)	0.9875 (0.05895)
voxel-by-voxel	0.2090 (0.00600)	0.2691 (0.00711)	0.3170 (0.01017)	0.3783 (0.01057)
spatio-temporal	0.0151 (0.00185)	0.0219 (0.00334)	0.0345 (0.00550)	0.0574 (0.00946)

with MBF_i^{true} the true MBF value in voxel i, $\widehat{MBF}_i$ the estimated MBF value, and N the number of all voxel of all three slices. Afterwards, the MSE values of all 50 simulations were summarized by median and standard deviation.

F. In vivo data acquisition

For *in vivo* evaluation, MRI perfusion data from six patients with coronary artery disease was used. A dual sequence approach was used to estimate the signal in the myocardium and in the LV blood pool accurately [26]. The images were acquired with a 0.1 mmol/kg injection of a Gadolinium-based contrast agent on a 1.5-T Siemens Sonata scanner with single-shot FLASH with 48×64 voxel resolution on a 30×40 *cm* field of view (FOV) with a short saturation recovery time of 3.4 msec, TE = 0.5msec, TR = 1 msec for measurement of the LV blood pool, followed by measurement in the same cardiac cycles with a 108×256 voxel resolution on the same FOV with a longer saturation recovery time of 63.4 msec, TE = 1.2 msec, TR = 1.86 msec for measurement of the LV myocardium. Each subject was scanned once under rest, followed by a scan after injection of 140 μg/minute/kg of adenosine for four minutes, *i.e.*, under stress [2]. For the myocardial signal, the regions of interest (ROI) were drawn by an expert radiologist. The ROIs were moved manually to follow any in-plane respiratory motion.

III. RESULTS

A. Simulation study A

Table I lists the MSE of estimated voxel-wise MBF values for the segment, the voxel-by-voxel, and the proposed spatio-temporal approach. For all simulations, the MSE is noticeably lower for the spatio-temporal approach compared with both the voxel-by-voxel and the segment approach. To explore the reliability of the different approaches the variance of the MSE in the 50 simulations is also given in Table I. The MSE naturally depends on the SNR, a lower SNR leads to a higher MSE. The highest MSE can be seen for the segment analysis and the variance of MSE is quite high, which indicates a low reliability of the estimation. The MSE for the voxel-by-voxel analysis is roughly ten times greater than the MSE of the spatio-temporal approach.

Fig. 1 depicts the true MBF values used in the simulation and the values estimated by the different approaches for one of the simulation runs with $SNR = 3$. In order to depict results acquired on voxel level we use a nested method similar to the bullseye representation for results on segment level [3]. The basal slice is depicted on the outside and the apical slice on the inside of the mid slice. Here, MBF values are underestimated by the voxel-by-voxel and the segment approach, which partially explains the higher MSE seen above. In particular, areas with higher true MBF values are underestimated by the voxel-by-voxel and the segment approach, for example in the mid

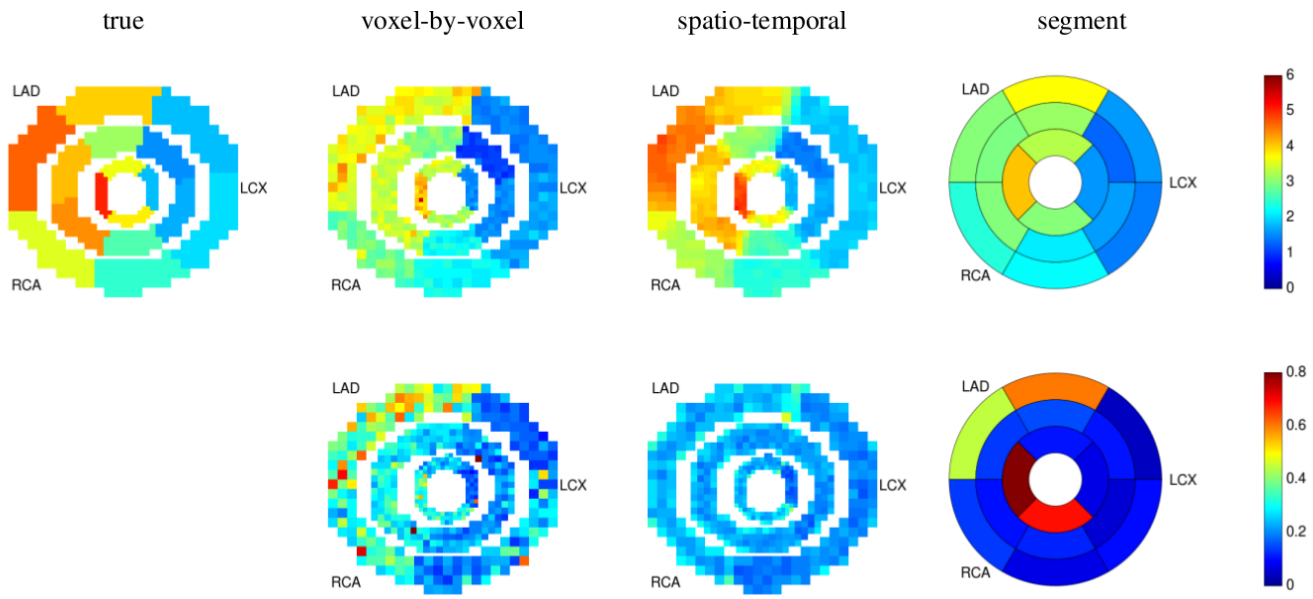

Fig. 2. Top row: True and estimated MBF values for one simulation run (SNR=3) of simulation B. Bottom row: IQR of estimated MBF for all three approaches.

TABLE II
SIMULATION B: MEAN SQUARED ERROR OF MBF; MEDIAN AND STANDARD DEVIATION (IN BRACKETS) OVER 50 SIMULATIONS, AT FOUR DIFFERENT NOISE LEVELS FOR ALL THREE APPROACHES.

SNR	4.25	3.00	2.12	1.50
segment	0.3616 (0.08204)	0.4964 (0.08682)	0.7029 (0.08006)	0.8132 (0.10658)
voxel-by-voxel	0.2652 (0.00734)	0.3267 (0.00794)	0.3750 (0.01216)	0.4297 (0.01402)
spatio-temporal	0.0400 (0.00286)	0.0549 (0.00451)	0.0744 (0.00757)	0.1072 (0.01191)

TABLE III
SPEARMAN'S CORRELATION COEFFICIENT FOR ESTIMATED MBF VALUES OF *in vivo* DATA SET.

patient	1		2		3		4		5		6	
scan	rest	stress	rest	stress	rest	stress	rest	stress	rest	stress	rest	stress
voxel—segment	0.068	0.328	0.352	0.551	0.297	0.592	0.260	0.143	0.514	0.117	0.447	0.142
voxel—spatial	0.821	0.813	0.860	0.815	0.773	0.856	0.623	0.709	0.714	0.385	0.296	0.130
segment—spatial	0.030	0.331	0.486	0.772	0.597	0.702	0.643	0.212	0.733	0.507	0.720	0.529

left anterior descending and right coronary artery segments.

The interquartile range IQR, as a measure of the uncertainty of MBF estimation, is also shown in Fig. 1. For the segment approach the IQR and, hence, the uncertainty is generally low, as the segment approach aggregates data. However, the IQR is rather high for three segments. The IQR for the spatio-temporal approach is relatively low compared to the voxel-by-voxel approach, due to the use of information from adjacent voxel.

B. Simulation study B

Fig. 2 depicts the true MBF values used in simulation B and the values estimated by the different approaches. This simulation assumes edges in the MBF profile. Although the spatio-temporal approach uses a smoothing technique, due to its adaptiveness the method is able to retain the edges in the MBF map. The edges can also be seen from the voxel-by-voxel MBF map, but with higher variability in the segments. Similar to simulation A, a slight underestimation of MBF values can be seen for the voxel-by-voxel and the segment approach. The IQR is also shown in Fig. 2, and the results are similar to the results in simulation A. The IQR is clearly reduced by the spatio-temporal approach compared to the voxel-by-voxel method, and the IQR for the segment technique is in general rather low, but quite high for four segments.

Table II lists the MSE of MBF estimation for the different levels of SNR. As above, the highest MSE can be seen for the segment estimation and the lowest MSE for the spatio-temporal approach. MSE is also higher for lower SNRs. The reliability, measured by the standard deviation, is similar to the reliability in simulation A.

C. In vivo study

The proposed approaches were evaluated on six patients with different types of stenosis with scans at rest and under stress. Table III lists the correlation (Spearman's coefficient) of MBF values per voxel estimated by the three different approaches for all scans. For the segment approach, the

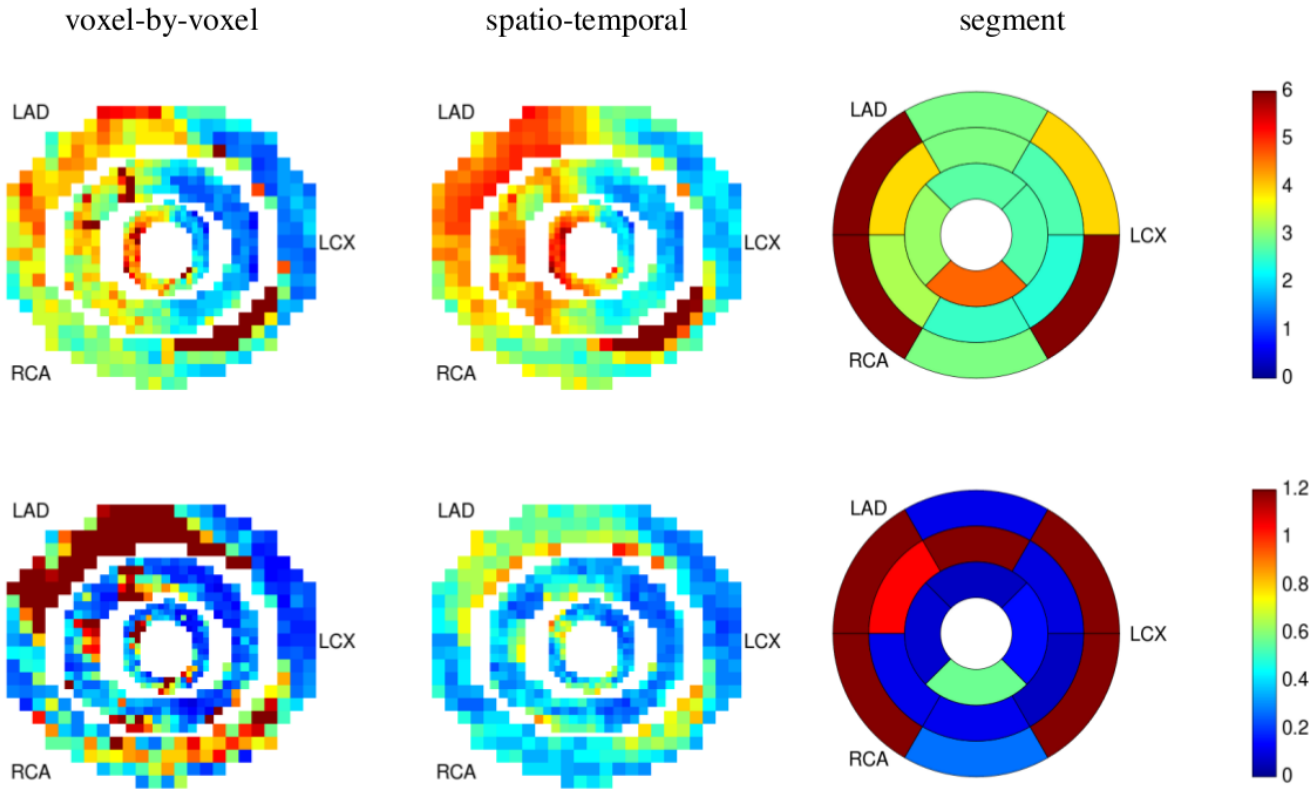

Fig. 3. Top row: Estimated MBF values for scan under stress of patient 3. Bottom row: Length of quartile range (IQR) of estimated MBF.

TABLE IV
MEDIAN IQR VALUES PER SCAN FOR *in vivo* DATA SET.

patient	1		2		3		4		5		6	
scan	rest	stress	rest	stress	rest	stress	rest	stress	rest	stress	rest	stress
segment	1.488	0.634	0.493	0.195	0.095	0.749	0.312	0.732	1.191	2.311	2.751	1.229
voxel-by-voxel	0.174	0.328	0.191	0.538	0.166	0.582	0.348	0.583	0.362	0.923	1.983	0.380
spatio-temporal	0.217	0.269	0.250	0.327	0.181	0.298	0.329	0.346	0.292	0.347	0.297	0.259

segment MBF was assigned to each voxel in the segment. MBF estimates acquired by the voxel-by-voxel and the spatio-temporal approach generally show a high correlation; for eight scans the correlation exceeds 0.7. Correlations between spatio-temporal and segment approach are typically lower compared with voxel-by-voxel/spatio-temporal correlations, but higher than correlations between voxel-by-voxel and segment approaches. The latter are noticeably low and do not exceed 0.592.

Table IV lists the median IQR of estimated MBF values. For the scans under stress, IQR values are in general increasing from spatio-temporal approach to voxel-by-voxel and to segment approach. For the scans at rest, for two scans each, one of the methods has the lowest IQR. The IQR values of the spatio-temporal approach are similar for all scans; they cover a range of 0.181 to 0.347. The range of median IQR values is 0.166 to 1.983 for the voxel-by-voxel method and 0.095 to 2.751 for the segment approach.

For patient 3, Fig. 3 depicts estimated MBF values along with the IQR values for the scan under stress. Voxel-by-voxel and spatio-temporal analysis both show a perfusion defect in the LCX area of all slices. The segment approach, however, overestimates the blood flow in this area. In the basal inferolateral segment the MBF maps estimated by the voxel-by-voxel and by the spatio-temporal approach indicate that the region of interest was not drawn properly for this segment and a couple of voxels actually belong to the LV blood pool. The segment approach cannot account for that and the MBF in this segment is overestimated. The IQR values for the voxel-by-voxel method in general exceed the IQR values for the spatio-temporal approach. In comparison, the IQR values for the segment approach are low for some of the segments and high for the others; the latter is in particular true for segments where the voxel-by-voxel and spatio-temporal methods show variability in MBF.

Fig. 4 depicts MBF maps and IQR maps for the scan at rest of patient 3. Here, voxel-by-voxel and spatio-temporal approach suggest blood flow is more or less similar for all areas in a slice, with increasing blood flow towards the apical slice. In contrast the segment approach shows noticeably high MBF values in some segments. The IQR map however shows, that the MBF estimate in these segments has rather high

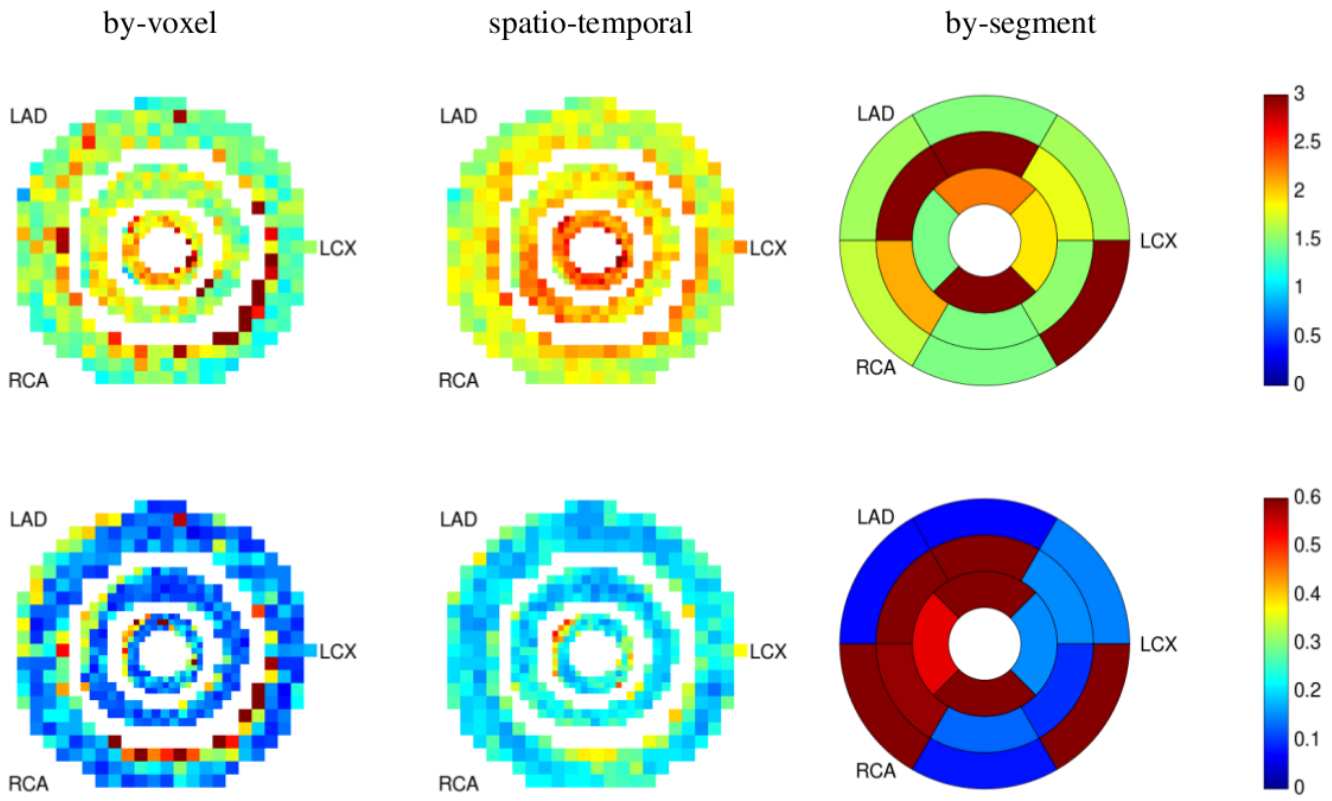

Fig. 4. Top row: Estimated MBF values for scan at rest of patient 3. Bottom row: Length of quartile range (IQR) of estimated MBF.

uncertainty, *i.e.*, a high IQR. The voxel-by-voxel IQR map shows some voxel with higher IQR, in particular at the edges of the myocardial tissue. The IQR of the spatio-temporal method is relatively low in all voxel.

As additional feature, the local smoothing parameters $\nu_{\{ij\}}$ can be mapped [17]. Fig. 5 depicts the estimated smoothing weights for the scan under stress of patient 3. The smoothing parameter is noticeably reduced towards the epicardium and endocardium, which is to be expected. Unlike [17] we do not have a large plane ROI. Rather the number of adjacent voxel is low towards epicardium and endocardium, so even a relatively low value of $\nu_{\{ij\}}$ has a larger influence on an epicardial or endocardial voxel i. The map shows regions where smoothing is locally reduced, for example in the inferolateral region where we assume a blood pool voxel in the ROI, or in the anterior region where defected and well-perfused tissue are adjacent.

Fig. 6 depicts MBF maps estimated by the spatio-temporal approach for the scans under stress of all other patients. All patients in this study had perfusion defects. For example, for patient 5 reduced perfusion can be seen in the LCX area of the basal and mid slice. For patient 2, however, perfusion is generally reduced for all areas. With the spatio-temporal approach, MBF maps can be derived in a robust way for all patients.

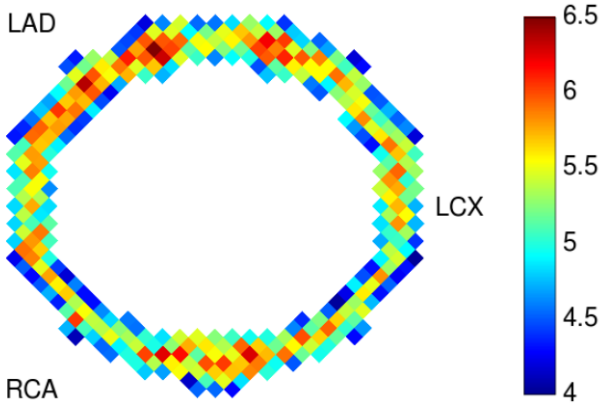

Fig. 5. Estimated local adaptive smoothing weights $\nu_{\{ij\}}$ for basal slice of scan under stress of patient 3.

IV. Discussion

In myocardial perfusion imaging, a voxel-by-voxel estimation procedure is susceptible to noise in the signal, and, hence, can be numerically unstable. In order to gain a numerically stable estimation technique, one has to introduce constraints. One possibility is to assume a certain shape of the residue curve [4], [27]. However, the kinetic processes in the tissue, and, hence, the shape of the residue curve, are not fully known. An alternative approach is to assume a smooth residue curve, modeled by a penalized B-spline [5]. Here, a constraint on the smoothness of the curve is introduced by penalizing the differences of the B-spline regression parameters. However, this is a rather weak constraint and has originally only been proposed for the analysis at the segment level. By introduc-

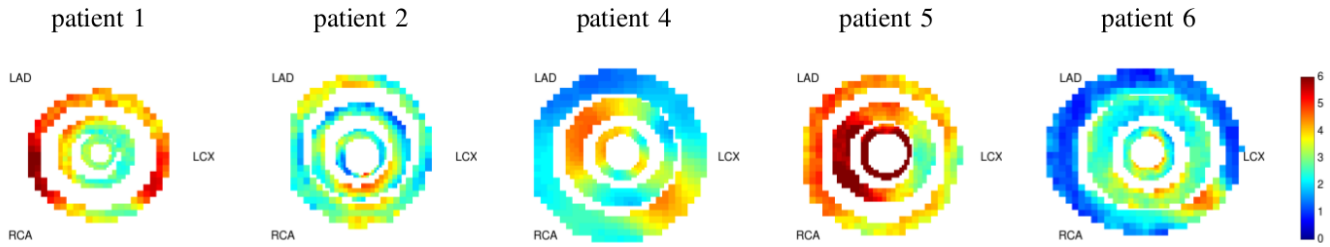

Fig. 6. MBF maps for scans under stress for all patients (except for for patient 3, who is shown in Fig. 3) estimated by spatio-temporal approach.

ing an additional spatial penalty on the B-spline regression parameter, we gain a robust algorithm for MBF estimation at the voxel level.

The local B-Spline model described in section II.A and II.B is similar to the model-free approach proposed by Jerosch-Herold *et al.* [5], however, it is formulated in a Bayesian framework. As Fahrmeir *et al.* [28] point out, point estimates are identical whether the regularization is formulated using a prior distribution or with a penalty. However, there are two differences in our approach compared to [5]. We use second-order differences, which implies slightly smoother curves, and we apply time-varying smoothing, which accommodates rapid changes in the response function.

We have presented a spatio-temporal model for a robust quantitative analysis of myocardial first-pass perfusion MRI scans. The proposed model combines temporal smoothing constraints with spatial information available from images. The proposed method combines the advantages of the two alternative approaches explored in this paper: Similar to the voxel-by-voxel method it provides MBF estimates per voxel, and, hence, is able to pick up local variance in perfusion. However, MBF estimates are more robust as, similar to the segment approach, information is spatially pooled.

Simulation results indicate that by averaging the signal per segment, one not only loses information on local micro-circulation, but also encourages under estimation of the blood flow. This is even more important in cases where there is high variability in blood flow in a segment, and even when the blood flow variability is low within a segment, inaccurate segmentation may perturb the result. Small errors in the segmentation process may "contaminate" the average signal per segment with either blood pool voxels or surrounding tissue and lead to biased estimates. Analysis at the voxel level does not suffer from segmentation problems and specific voxel that are not part of the myocardial tissue can be identified.

We used a Bayesian framework for all approaches, which allows one to quantify the uncertainty in MBF estimation. The Bayesian MCMC algorithm provides a posterior pdf for each MBF parameter. From this, not only point estimates for MBF can be computed (we used the median throughout this paper), but also interval estimators or even statistical tests are available. Here, we used the length of the interquartile range (IQR) to quantify the uncertainty. It is well known that MCMC algorithms have relatively long computation times. By using efficient algorithms, parameter estimation in the spatio-temporal model takes three to five minutes for a single slice, depending on the number of voxels. Using simple computation parallelization, the complete analysis may be performed in approximately six to seven minutes on a standard quad-core PC.

Both in the simulations and in the *in vivo* data sets the IQR for MBF estimates from the spatio-temporal approach was relatively low, and it was similar over all scans, whereas the IQR had higher variability for both the segment and voxel-by-voxel approach. That is, the estimates gained from the spatio-temporal approach are much more stable and the approach is more robust. The segment approach typically produces stable estimates only if the perfusion is similar throughout the segment. In cases where only parts of a segment are affected by a perfusion defect, the segment approach has high uncertainty in MBF estimation. For the voxel-by-voxel approach the IQR showed high variability, as the performance of this estimation procedure strongly depends on the noise in the signal.

An important feature of the proposed spatio-temporal approach is the neighbourhood structure. Assuming a global spatial smoothness is not appropriate for medical images. Locally adaptive smoothing allows one to retain sharp features and borders of myocardial tissue areas, *e.g.*, between segments. Adaptive estimation of local smoothing parameters can, however, only be done in a Bayesian framework. The benefits from such a framework include the fact that the local smoothing parameters can be mapped and information about edges in the tissue can be derived from such a map.

Here, motion correction was done manually. For clinical practice, an automatic registration step for correcting motion should be added as a pre-processing step, *e.g.* [29], [30]. Automatic registration methods could also be used to register scans at rest and under stress. From this, the myocardial perfusion reserve (MPR), given as the ratio of MBF under stress and MBF at rest, can be computed.

In summary, an analysis of myocardial perfusion MRI at the voxel level can provide additional information to the standard segment analysis used in first-pass perfusion cardiovascular MRI. The insight into local differences in the impulse response function may provide further information about the blood supply of the myocardial tissue and enhance the clinical value of perfusion cardiovascular MRI. By including spatial information and, hence, "borrowing strength" from adjacent voxel, the proposed spatio-temporal approach allows a more robust assessment of myocardial blood flow at the voxel level. In this paper, we explored the feasibility of such an

approach. Additional clinical studies comparing the results of the proposed approach with accepted clinical standards should be performed to further explore the practical clinical value of this methodology.

ACKNOWLEDGEMENTS

In vivo data were graciously provided by Peter Gatehouse, Cardiovascular Magnetic Resonance Unit, Royal Brompton Hospital, London, United Kingdom. We thank the reviewers for their critical and helpful comments.

REFERENCES

[1] J. R. Panting, P. D. Gatehouse, G.-Z. Yang, F. Grothues, D. N. Firmin, P. Collins, and D. J. Pennell, "Abnormal subendocardial perfusion in cardiac syndrome X detected by cardiovascular magnetic resonance imaging." *The New England journal of medicine*, vol. 346, no. 25, pp. 1948–53, 2002.

[2] M. Jerosch-Herold, R. T. Seethamraju, C. Swingen, N. M. Wilke, and A. E. Stillman, "Analysis of myocardial perfusion MRI," *Journal of Magnetic Resonance Imaging*, vol. 19, no. 6, pp. 758–770, 2004.

[3] M. D. Cerqueira, N. J. Weissman, V. Dilsizian, A. K. Jacobs, and S. Kaul, "Standardized Myocardial Segmentation and Nomenclature for Tomographic Imaging of the Heart: A Statement for Healthcare Professionals From the Cardiac Imaging Committee of the Council on Clinical Cardiology of the American Heart Association," *Circulation*, vol. 105, no. 4, pp. 539–542, 2002.

[4] T. A. Goldstein, M. Jerosch-Herold, B. Misselwitz, H. Zhang, R. J. Gropler, and J. Zheng, "Fast mapping of myocardial blood flow with MR first-pass perfusion imaging," *Magnetic Resonance in Medicine*, vol. 59, no. 6, pp. 1394–1400, 2008.

[5] M. Jerosch-Herold, C. Swingen, and R. T. Seethamraju, "Myocardial blood flow quantification with MRI by model-independent deconvolution," *Medical Physics*, vol. 29, no. 5, p. 886, 2002.

[6] P. H. C. Eilers and B. D. Marx, "Flexible smoothing with B-splines and penalties (with comments and rejoinder)," *Statistical Science*, vol. 11, no. 2, pp. 89–121, 1996.

[7] P. R. Johnston and R. M. Gulrajani, "Selecting the corner in the L-curve approach to Tikhonov regularization," *IEEE Transaction on Biomedical Engineering*, vol. 47, no. 9, pp. 1293–1296, 2000.

[8] B. D. Marx and P. H. C. Eilers, "Direct generalized additive modeling with penalized likelihood," *Computational Statistics & Data Analysis*, vol. 28, no. 2, pp. 193–209, 1998.

[9] A. Brezger, L. Fahrmeir, and A. Hennerfeind, "Adaptive Gaussian Markov random fields with applications in human brain mapping," *Journal of the Royal Statistical Society: Series C (Applied Statistics)*, vol. 56, no. 3, pp. 327–345, 2007.

[10] V. J. Schmid, B. Whitcher, A. R. Padhani, and G.-Z. Yang, "Quantitative analysis of Dynamic contrast-enhanced MR images based on Bayesian P-Splines," *IEEE Transactions on Medical Imaging*, vol. 28, no. 6, pp. 789–798, 2009.

[11] V. J. Schmid, P. D. Gatehouse, and G.-Z. Yang, "Attenuation Resilient AIF Estimation Based on Hierarchical Bayesian Modelling for First Pass Myocardial Perfusion MRI," in *Medical Image Computing and Computer-Assisted Intervention - MICCAI 2007*, N. Ayache, S. Ourselin, and A. Maeder, Eds. Berlin: Springer, 2007, pp. 393–400.

[12] K. Held, E. Rota Kops, B. J. Krause, W. Wells, R. Kikinis, and H. W. Muller-Gartner, "Markov random field segmentation of brain MR images," *IEEE Transactions on Medical Imaging*, vol. 16, no. 6, pp. 878–886, 1997.

[13] C. Gössl, D. P. Auer, and L. Fahrmeir, "Bayesian Spatiotemporal Inference in Functional Magnetic Resonance Imaging," *Biometrics*, vol. 57, no. 2, pp. 554–562, 2001.

[14] W. D. Penny, N. J. Trujillo-Barreto, and K. J. Friston, "Bayesian fMRI time series analysis with spatial priors," *NeuroImage*, vol. 24, no. 2, pp. 350–362, 2005.

[15] M. W. Woolrich, M. Jenkinson, J. M. Brady, and S. M. Smith, "Fully Bayesian spatio-temporal modeling of FMRI data," *IEEE Transactions on Medical Imaging*, vol. 23, no. 2, pp. 213–231, 2004.

[16] Q. Williams, J. A. Noble, A. Ehlgen, and H. Becher, "Tissue perfusion diagnostic classification using a spatio-temporal analysis of contrast ultrasound image sequences." in *Information processing in medical imaging*, G. E. Christensen and M. Sonka, Eds., vol. 19. Springer, Berlin, 2005, pp. 222–33.

[17] V. J. Schmid, B. Whitcher, A. R. Padhani, N. J. Taylor, and G.-Z. Yang, "Bayesian methods for pharmacokinetic models in dynamic contrast-enhanced magnetic resonance imaging." *IEEE Transactions on Medical Imaging*, vol. 25, no. 12, pp. 1627–36, 2006.

[18] S. Heim, L. Fahrmeir, P. H. C. Eilers, and B. D. Marx, "3D space-varying coefficient models with application to diffusion tensor imaging," *Computational Statistics & Data Analysis*, vol. 51, no. 12, pp. 6212–6228, 2007.

[19] V. J. Schmid and G.-Z. Yang, "Spatio-Temporal Modelling of First-Pass Perfusion Cardiovascular MRI," in *World Congress on Medical Physics and Biomedical Engineering, September 7-12, 2009, Munich, Germany*. Springer, 2009, pp. 45–48.

[20] H. Rue and L. Held, *Gaussian Markov Random Fields: Theory and Applications (Monographs on Statistics and Applied Probability)*. Chapman & Hall, 2005.

[21] D. G. Clayton, "Generalized linear mixed models," pp. 275–301, 1996.

[22] J. E. Besag and D. M. Higdon, "Bayesian analysis of agricultural field experiments," *Journal of the Royal Statistical Society. Series B (Statistical Methodology)*, vol. 61, no. 4, pp. 691–746, 1999.

[23] W. R. Gilks, S. Richardson, and D. J. Spiegelhalter, *Markov Chain Monte Carlo in Practice*. London: Chapman & Hall, 1996.

[24] D. Bates and M. Maechler, *Matrix: Sparse and Dense Matrix Classes and Methods*, 2010, R package version 0.999375-45. [Online]. Available: http://CRAN.R-project.org/package=Matrix

[25] R Development Core Team, *R: A Language and Environment for Statistical Computing*, R Foundation for Statistical Computing, Vienna, Austria, 2010, ISBN 3-900051-07-0. [Online]. Available: http://www.R-project.org

[26] P. D. Gatehouse, A. G. Elkington, N. A. Ablitt, G.-Z. Yang, D. J. Pennell, and D. N. Firmin, "Accurate assessment of the Arterial Input Function during High-Dose Myocardial Perfusion Cardiovascular Magnetic Resonance," *Journal of Magnetic Resonance Imaging*, vol. 20, pp. 39–45, 2004.

[27] M. Jerosch-Herold, X. Hu, N. S. Murthy, C. Rickers, and A. E. Stillman, "Magnetic resonance imaging of myocardial contrast enhancement with MS-325 and its relation to myocardial blood flow and the perfusion reserve." *Journal of Magnetic Resonance Imaging*, vol. 18, no. 5, pp. 544–54, 2003.

[28] L. Fahrmeir, T. Kneib, and S. Konrath, "Bayesian regularisation in structured additive regression: a unifying perspective on shrinkage, smoothing and predictor selection," *Statistics and Computing*, vol. 20, no. 2, pp. 203–219, 2009.

[29] L. M. Bidaut and J. P. Vallée, "Automated registration of dynamic MR images for the quantification of myocardial perfusion." *Journal of Magnetic Resonance Imaging*, vol. 13, no. 4, pp. 648–55, 2001.

[30] J. Milles, R. van der Geest, M. Jerosch-Herold, J. Reiber, and B. Lelieveldt, "Fully automated registration of first-pass myocardial perfusion mri using independent component analysis," in *Information Processing in Medical Imaging*, ser. Lecture Notes in Computer Science, N. Karssemeijer and B. Lelieveldt, Eds. Springer Berlin, 2007, vol. 4584, pp. 544–555.